Annexure – III

FABRICATION OF NANOSENSORS FOR REACTOR APPLICATIONS

(File.No.40-74/2011 (SR) Dt.05.07.2011)

Project Completion Report
for the period 01.07.2011 to 31.12.2014

Submitted to

UNIVERSITY GRANTS COMMISSION
BAHADUR SHAH ZAFAR MARG
NEW DELHI – 110 002

By
Dr. R.ILANGOVAN

Principal Investigator- UGC-MRP

Annexure – IX

UNIVERSITY GRANTS COMMISSION
BAHADUR SHAH ZAFAR MARG
NEW DELHI – 110 002

PROFORMA FOR SUBMISSION OF INFORMATION AT THE TIME OF SENDING THE FINAL REPORT OF THE WORK DONE ON THE PROJECT

1. Title of the Project: 'Fabrication of Nanosensors for Reactor Applications'
2. NAME AND ADDRESS OF THE: PRINCIPAL INVESTIGATOR
Dr. R. ILANGOVAN,
Assistant Professor (Formerly),
Department of Nanoscience and Technology,
Alagappa University,
Karaikudi – 630 003.
3. NAME AND ADDRESS OF THE INSTITUTION: **Alagappa University, Karaikudi – 630 003.**
4. UGC APPROVAL LETTER NO. AND DATE: F.No.40 – 74 /2011 (SR), Dated 05.07.2011
5. DATE OF IMPLEMENTATION: 01.07.2011
6. TENURE OF THE PROJECT: 01.07.2011 to 31.12.2014
7. TOTAL GRANT ALLOCATED : **Rs.9,34,933/-**
8. TOTAL GRANT RECEIVED : **Rs.8,64,920/-**
9. FINAL EXPENDITURE : **Rs.8,51,895/-**
10. TITLE OF THE PROJECT : **'Fabrication of Nanosensors for Reactor Applications'**
11. OBJECTIVES OF THE PROJECT

- To prepare nanocrystalline Titanium Oxide and Zinc Oxide thin films by sol gel spin coating and dip coating techniques.
- To study the effect of La, W and Nb doping of the thin films.
- The structural, morphological and thermal properties of the prepared thin films are to be determined by employing XRD, SEM and TGA/DTA analyses.
- To study the Hydrogen and Oxygen gas sensing properties of the prepared thin films through the change of film conductivity upon the exposure of target gas at room temperature.

12. WHETHER OBJECTIVES WERE ACHIEVED

(GIVE DETAILS)

- TiO_2 nanoparticles have been synthesized by sol gel process using *Aloe vera* plant extract as a biological agent.
- Thermal, Structural, Morphological and Elemental properties of the synthesized TiO_2 and ZnO nanomaterials have been studied by TGA/DTA, XRD, FESEM, TEM and EDAX analysis respectively.
- The indigenous gas sensor experimental set up consisting of Keithley Picoammeter (Model 6487), Temperature controller, Glass chamber, sample heating set up and vacuum pump **(Fig.1)** was designed as one of the outcomes under this project.

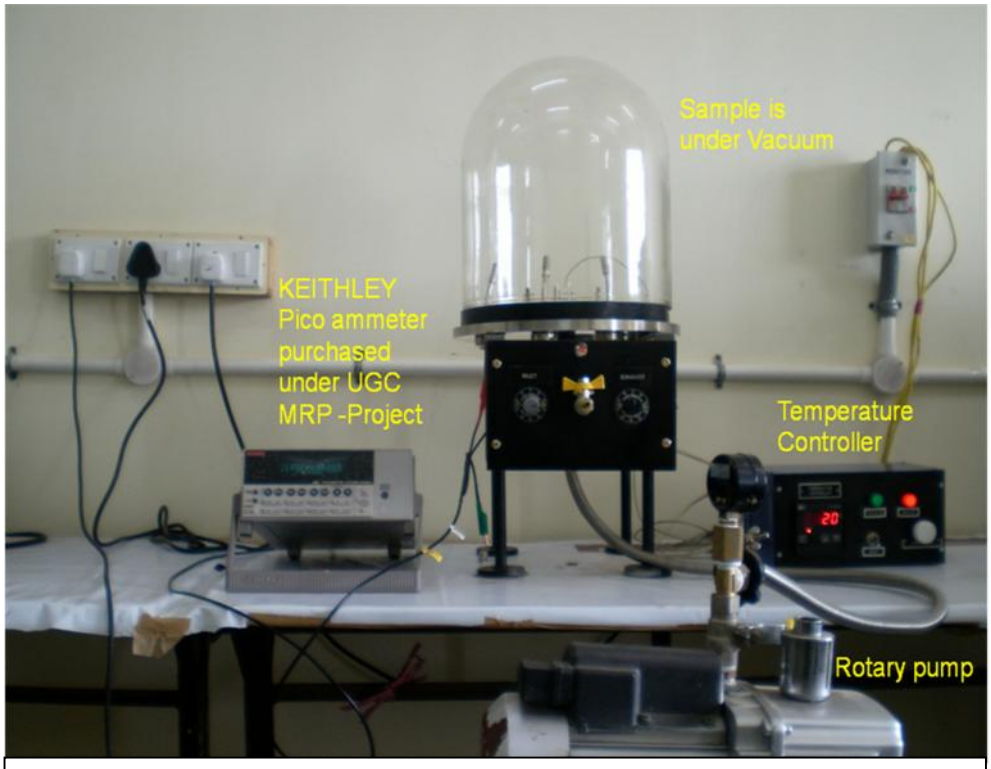

Fig. 1: Indigenous gas sensor experimental set up

- Pure and different concentration (1, 3, 5 and 10 wt%) of La incorporated ZnO thin films with novel nanocorn morphology were prepared by means of sol gel dip coating technique onto glass substrates. The prepared thin films were subjected to TGA/DTA, XRD, Thickness measurement, FESEM and EDAX characterizations.

- Gas sensing property of pure and La:ZnO thin films have been studied against 1000 ppm of H_2 gas at room temperature.

13. ACHIEVEMENTS FROM THE PROJECT

- ✓ Pure and La incorporated ZnO thin films with novel nanocorn morphology was prepared by Sol Gel dip coating technique.

- ✓ The prepared La incorporated ZnO thin films showed maximum sensitivity of S≈ 60% towards 1000 ppm of H_2 gas at **Room Temperature**.

- ✓ TiO_2 nanoparticles with novel nanocoral morphology was synthesized by Sol Gel method using *Aloe vera* plant extract as biological agent.

- ✓ *Aloe vera* plant extract showed a great impact on the structural, morphological and also phase transformation of TiO_2 (from Anatase to Rutile) nanoparticles.

- ✓ A project fellow Mr. K.S. Venkatesh has been awarded to Ph.D.

- ✓ Based on the obtained results, two papers were published in peer reviewed international journals with due acknowledgement to UGC.

14. SUMMARY OF THE FINDINGS

(IN 500 WORDS)

Pure and La (1, 3, 5 and 10 wt %) incorporated ZnO thin films were prepared by sol gel dip coating technique. Simultaneous TGA/DTA analysis was performed to study the thermal behaviour of the xerogel of pure ZnO solution and it revealed the formation of metal oxide (ZnO) takes place at around 350^{o}C and the XRD results emphasized the same.

The powder X-ray diffractogram revealed the presence of well crystalline ZnO thin films belongs to the hexagonal structure with polycrystalline nature. XRD pattern shows that the c-axis orientation is not exhibited for pure and at lower concentration of La (1 wt %), and the growth of the film takes place towards c- axis orientation from 3 wt % of La incorporation onwards. Hence, the incorporation of 3 wt % and above concentration of La increases the growth of ZnO thin film towards c-axis as a preferential orientation of (002) plane, i.e. perpendicular to the substrate. The thickness of the prepared thin films was measured using Stylus Profiler and the thickness of pure, 1, 3, 5 and 10 wt% of La incorporated ZnO thin films were found to be 1.41, 1.32, 1.19 1.08 and 1.02 μm.

FESEM images were clearly visualized the presence of nanocorns composed of very small and well defined tiny particles ranging between 15 and 20 nm. The presence of Zn, O and La elements were observed through EDX analyses and no other elements were detected in the spectra.

The variation of resistivity with respect to time for pure and La (1, 3, 5 and 10 wt%) incorporated ZnO thin films towards 1000 ppm of H_2 gas concentration at room temperature was studied. Pure ZnO thin film showed a decrease in the resistivity upon exposing the hydrogen gas and sensitivity was good (S=51%) at room temperature.

A novel TiO_2 nanocoral architecture was obtained first time using a*loe vera* plant extract as a bio-capping agent by sol gel process. The concentration variation of a*loe vera*

plant extract enormously changes the particle size of TiO_2 nanopowder and thereby it leads to control the particle size. XRD results substantiated that the phase (Anatase and Rutile) transformation of TiO_2 nanoparticle depends on the concentration of a*loe vera* plant extract. FT Raman spectra emphasized the presence of TiO_2 anatase phase and the Raman band shiftted with respect to the particle size variation. FTIR spectra clearly indicate the biological molecules which are responsible for the formation of TiO_2 nanoparticles. The surface area was measured by BET analysis and it is to be 27.6238 m^2 /g. SEM images depicted the particles homogeneity and the reduction of particle size with respect to the concentration of a*loe vera* plant extract. Furthermore, TEM images demonstrated the plausible nanocorals decorated with the nanopolyps having the diameter in the range of 15-30 nm.

15. CONTRIBUTION TO THE SOCIETY

(GIVE DETAILS)

- Gas sensors operable at room temperature are having a very high demand. Since, the Hydrogen gas has low ignition velocity, it can easy fire if there is an increase in the temperature. Hence, Sensors working under operating temperature is not suitable for H_2 gas sensing. Also, working of sensor device in the reactors under operating temperature is difficult.

- Based on the above requirement, ZnO thin film was coated on the glass substrate and evaluated for sensing H_2 gas at room temperature. The prepared pure ZnO thin film showed good response to the H_2 gas (S=51%) at room temperature.

- The outcome of the project has been arrived as 02 International papers in the peer reviewed journal.

16. WHETHER ANY Ph.D. ENROLLED/PRODUCED OUT OF THE PROJECT

PhD produced : **01**

Manpower trained : **01**

17. NO. OF PUBLICATIONS OUT OF THE PROJECT - **02**

(List and Full papers attached)

S.No	Title of the Article	Authors	Name of the journal Vol. No. &Page	Impact factor
1	Fabrication of room temperature H2 gas sensor using pure and La: ZnO with novel nanocorn morphology prepared by sol–gel dip coating method.	K.S.Venkatesh, K.Vijayalakshmi, K.Karthick , S.R.Krishnamoorthi, N.S.Palani, R.Ilangovan.	J Mater Sci: Mater Electron (2014) 25:4339–4347 DOI 10.1007/s10854-014-2171-0	2.195
2	Facile one step synthesis of novel TiO_2 nanocoral by sol-gel method using Aloe vera plant extract.	K.S.Venkatesh, S.R.Krishnamoorthi, N.S.Palani, V.Thirumal, Sujin P.Jose, Fu-Ming Wang and R.Ilangovan.	Indian J Phys, May 2015, Volume 89, Issue 5, pp 445-452, ISSN No. 0974-9845.	1.407

PRINCIPAL INVESTIGATOR

REGISTRAR

REGISTRAR
ALAGAPPA UNIVERSITY
KARAIKUDI

J Mater Sci: Mater Electron (2014) 25:4339–4347
DOI 10.1007/s10854-014-2171-0

Fabrication of room temperature H_2 gas sensor using pure and La: ZnO with novel nanocorn morphology prepared by sol–gel dip coating method

K. S. Venkatesh · K. Vijayalakshmi · K. Karthick · S. R. Krishnamoorthi · N. S. Palani · R. Ilangovan

Received: 18 June 2014 / Accepted: 11 July 2014 / Published online: 22 July 2014

Abstract Nanostructured ZnO thin films with different lanthanum concentration (0, 1, 3, 5 and 10 wt%) were fabricated by sol–gel dip coating method on glass substrates. The effect of La incorporation on structural, morphological and H_2 gas sensing (room temperature) properties of the ZnO thin films was studied. Thermal behaviour of the xerogel of pure ZnO was studied by thermo gravimetric analysis/differential thermal analysis. The structural property of the films was analyzed by powder X-ray diffraction method and which revealed the presence of hexagonal structure. It emphasized that the film became (002) textured upon the 3 wt% of La incorporation onwards. The surface morphology was examined by field emission scanning electron microscopy equipped with energy dispersive X-ray spectroscopy (EDX) and it substantiated that all the films have uniform distribution of particles with novel corn like morphology. Obviously, the length of nanocorn increases with the increase of La. The elemental composition was studied by EDX spectroscopy. Photoluminescence (PL) spectra revealed that La: ZnO thin films showed a blue shift and an enhanced PL intensity over that of the pure ZnO. The H_2 gas sensitivity of the pure and La: ZnO thin films were studied towards the concentration of 1,000 ppm. 1 wt% of La incorporated ZnO thin film showed a high sensitivity (51 %) than the pure and the higher La concentration. The increase and decrease of H_2 gas sensitivity of pure ZnO upon La incorporation is also discussed in this paper.

K. S. Venkatesh · S. R. Krishnamoorthi · N. S. Palani · R. Ilangovan (✉)
Nanoelectronics Laboratory, Department of Nanoscience and Technology, Alagappa University, Karaikudi 630 004, Tamil Nadu, India
e-mail: rajangamilangovan@gmail.com

K. Vijayalakshmi · K. Karthick
Research Department of Physics, Bishop Heber College, Tiruchirapalli 620 017, Tamil Nadu, India

1 Introduction

The usage of hydrogen (H_2) is rapidly increasing day by day and simultaneously, the occurrence of hazards is also increasing associated with the hydrogen namely respiratory ailment, component failure, ignition and burning. Due to its minimum ignition energy (0.017 mJ) even in air atmospheric pressure, H_2 easily get ignited and it has high burning velocity also. Upon long term preservation of the H_2 gas, many metals and plastics can lose its ductility and strength which leads to the formation of cracks and can eventually cause rupture thereby hydrogen leakage will takes place. Moreover, H_2 is also used in metal smelting, glass making, petroleum extraction, etc. [1]. Hydrogen gas is a colorless, odorless, and not detectable by human senses. It is lighter than air and highly difficult to detect unless accumulation occurs. It is also important to monitor/control the hydrogen concentration in nuclear reactors, coal mines and semiconductor manufacturing [2–4]. In order to avoid hazards caused by H_2, fast and highly sensitive H_2 gas sensors to operate at room temperature should be developed. Certain metal oxides have proved their potential applications in the field of gas sensors and to name a few are ZnO, TiO_2, SnO_2, In_2O_3, and WO_3 etc. Among the semiconducting metal oxides, ZnO is a promising candidate for H_2 gas sensors and it posses more oxygen vacancies which recognize more adsorption of a target gas [5, 6]. In addition, ZnO is being potentially used in various applications such as solar cells [7], sensors [8, 9], antimicrobial activity [10], Drug release carrier [11], Hydrogen

sensor [12–14], LPG sensing [15], Transparent conductive oxide thin films [16] etc. A modification by means of doping using foreign materials in ZnO lattice can improve the microstructure of the material including grain size, growth kinetics, and surface morphology; thereby it leads towards enhanced properties for gas sensing [17]. ZnO nanoparticles can be synthesized by different methods such as microwave assisted hydrothermal method [18], sol–gel [19], biosynthesis [10, 20], co-precipitation method [21] etc. In the case of metal oxide nanopowder for gas sensor applications, already synthesized and calcined nanopowder is coated onto the surface of the ceramic tube or substrate by paint brushing technique and again heat treated at higher temperature for the removal of chemical binding agent as well as for the adhesion with the coated solid support [22, 23]. The two fold heat treatment can leads to some faults such as non uniform coating, agglomeration and some time cracking and peeling off too. These may affect the grain boundaries of the metal oxide nanoparticles and thereby worsen the gas sensing ability. In order to overcome this problem, thin films based semiconducting metal oxides are being preferred because it provides more opportunities to strengthen gas sensors by means of controlling the film thickness, uniformity, choice of substrates because substrates are playing a pivotal role in gas sensors [24] and mainly one time heat treatment associated with the thin film preparation. Nanostructured ZnO thin films can be prepared by various techniques including dip coating [25], spin coating and sputtering [26, 27] and so on. Dip coating method offers several advantages such as ambient preparation conditions, coating on large area as well as complicated solid support (e.g. alumina tube) and mainly low cost. In this present communication, the preparation of pure and La incorporated ZnO thin films by sol–gel dip coating method is reported and the prepared thin films have been characterized by thermo gravimetric-differential thermal analysis (TGA/DTA), powder XRD analysis, field emission scanning electron microscopy (FESEM). The effect of La incorporation on the structural, morphological and hydrogen gas sensing performance of ZnO at room temperature are studied. In the present work, pure ZnO showed good sensitivity at room temperature, when compared with the previous report [28]. Also lower concentration of La incorporation enhances the sensitivity compared to pure ZnO. The higher concentration of La decreases the sensitivity and the variation of sensitivity with La incorporation is discussed in this report.

2 Experimental

Pure and different concentration (1, 3, 5 and 10 wt%) of La incorporated ZnO precursor solutions were prepared by sol–gel method. Zinc acetate dihydrate [Zn $(CH_3COO)_2{\cdot}2H_2O$] was dissolved in 2-Methoxy ethanol to obtain the concentration of the solution for 0.1 M. The solution was vigorously stirred for 3 h to obtain clear and homogeneous solution under ambient temperature. In order to stabilize the sol, an appropriate quantity of diethanolamine was added in the solution during stirring process. Furthermore, the stirred solution was sonicated for 20 min. The precursor was used for the preparation of pure ZnO thin films. In the preparation of La: ZnO precursor solution, Lanthanum nitrate hexahydrate [La $(NO_3)_3{\cdot}6H_2O$] was appropriately added to Zn $(CH_3COO)_2{\cdot}2H_2O$ and 2-Methoxy ethanol solution in the beginning. Then the further process is same as pure ZnO preparation. Thus prepared precursor solutions were used for the fabrication La incorporated ZnO thin films.

In order to improve the adhesion property of thin films, substrates (glass slides) were immersed in hydrofluoric acid (HF) diluted in deionized water (1:9 ratios) for 15 s. Then the glass slides were cleaned with soap oil and deionized water. After that the glass slides were cleaned using sonicator in acetone bath followed by deionized water for the removal of the presence of HF content in the cavity of the substrate and finally the glass slides were cleaned with isopropyl alcohol to remove the presence of any organic impurities and dried in a hot air oven.

The cleaned glass slides and prepared pure and La: ZnO precursor solutions were used for thin film preparation by dip coating method. The deposition was performed by immersing the glass substrate in the precursor solution with a controlled withdrawal speed of 1 mm/s in an ambient atmosphere and consecutively immersed in the double distilled (DD) water (90 °C). After each deposition, the film was dried at 100 °C for 30 min and the same process was repeated for 10 times to increase the thickness of the film. Finally, the fabricated thin films were subjected to annealing at 350 °C for 1 h in tubular furnace with the heating rate of 2 °C/min.

The thermal property of the xerogel of pure ZnO solution with respect to temperature was studied by TGA/DTA using (Model: STA 409 PL Luxx) under N_2 gas atmosphere from 30 to 900 °C with a heating rate of 10 °C/min. The XRD patterns of the pure and La: ZnO thin films were recorded by Cu Kα radiation with the wavelength of 1.54060 Å using X'PERT PRO (PANalytical) diffractometer system. The thickness of the prepared pure and La: ZnO thin films were measured using Mitutoyo surface profilometer (SJ-301). The surface morphology and chemical composition of the deposited thin films were examined by FESEM equipped with energy dispersive X-ray spectroscopy (EDX) (Model: Hitachi S-4500). Photoluminescence spectra were recorded in the wavelength range from 350 to 600 nm with an excitation wavelength of

320 nm using photoluminescence spectrometer (Varian Cary Eclipse).

The indigenously made gas sensor experimental set up was used for the H_2 gas sensor experiment. The thin film was mounted on the substrate holder within the glass chamber having the gas inlet and outlet valves. The required concentration of hydrogen gas was allowed inside the glass chamber using mass flow controllers (MFC). An ohomic contacts were made on the films using silver paste (negligible contact resistance). In order to measure the variation of electrical resistivity upon the gas exposure, two leads were taken out from the ohmic contacts and connected to the Keithley 6487 Picoammeter/Voltage source. The sensitivity (S) was calculated using the following relation [29]:

$$S = \frac{R_a - R_g}{R_a} \times 100 \quad (1)$$

where, R_a and R_g are the electrical resistivity of the sensor in the presence of air and in test gas respectively.

3 Results and discussion

Simultaneous TGA/DTA analysis was performed to study the thermal behaviour of the xerogel of pure ZnO solution and shown in Fig. 1a. A weight loss at 100 °C is attributed to the elimination of physisorbed and chemisorbed water molecules. In DTA curve a broad exothermic region from 100 to 300 °C is ascribed to the decomposition of reacted organic matter such as 2-Methoxy ethanol, diethanolamine. Furthermore, the formation of metal oxide (ZnO) takes place at around 350 °C and the XRD results emphasized the same.

The powder X-ray diffractograms revealed that the well crystallized ZnO thin films belongs to the hexagonal structure with polycrystalline nature is observed (Fig. 1b) and matched with the standard data (JCPDS File No. 89-0510). From the XRD data the average crystallite size was estimated using Scherrer equation (Eq. 2), (where 0.9 is a constant, λ is the wavelength of X-ray source, β is the full width at the half maximum in radians, θ is the Bragg's diffraction angle) and the estimated average crystallite size of the pure, 1, 3, 5 and 10 wt% of La incorporated ZnO thin films were 37, 33, 30 29.5 and 27 nm respectively. It can be obviously seen from the XRD patterns that the c-axis orientation is not exhibited for pure and at lower concentration of La (1 wt%), and the growth of the film takes place towards c-axis orientation from 3 wt% of La incorporation onwards. Hence, the incorporation of 3 wt% and above concentration of La increases the growth of ZnO thin film towards c-axis as a preferential orientation of (002) plane, i.e. perpendicular to the substrate [30]. Upon La addition, the position of the (002) plane is shifted towards lower angles (2θ) and also it expands the ZnO lattice along c-axis due to the lattice mismatch between La and ZnO lattice.

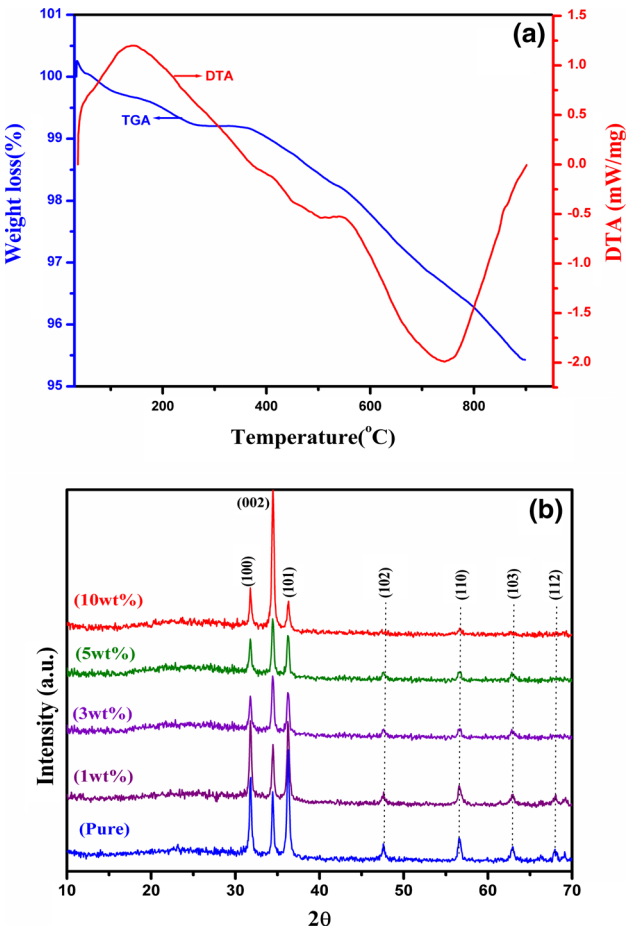

Fig. 1 **a** TGA/DTA analysis of pure ZnO xerogel. **b** XRD patterns of pure and La: ZnO thin films

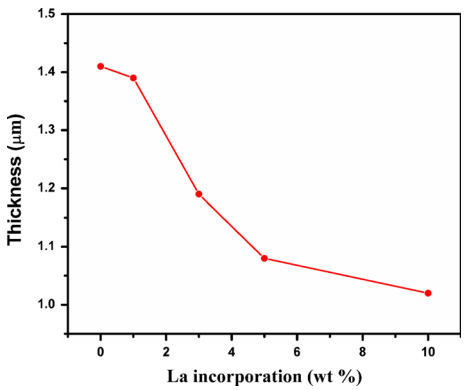

Fig. 2 Thickness of pure, 1, 3, 5 and 10 wt% of La incorporated ZnO thin films

$$D = \frac{0.9\lambda}{\beta \cos\theta} \quad (2)$$

The thickness of the prepared thin films was measured using Stylus Profiler and presented in Fig. 2. As seen from this Fig. 2, the thickness of pure, 1, 3, 5 and 10 wt% of La incorporated ZnO thin films were found to be 1.41, 1.32, 1.19 1.08 and 1.02 μm and the appropriate growth rates are 0.141, 0.132, 0.119, 0.108 and 0.102 μm respectively. The decrease in the film thickness upon La incorporation is clearly observed and also similar characteristics were observed for Mn doped ZnO thin films [31].

The impact of La doping on the surface morphology of the ZnO thin films was examined. The FESEM images of pure and La incorporated ZnO thin films are apparently showing the novel corn-like morphology (Fig. 3a–c). FESEM images are clearly visualizing the presence of nanocorns composed of very small and well defined nanoparticles ranging from 15 to 20 nm. As seen from the images, the length of the ZnO nanocorns augments upon La doping which implies the longitudinal growth of nanostructures. This is pertaining to the expansion of ZnO lattice towards c-axis and this phenomenon is consistent with the XRD results.

The elemental composition of the prepared thin films was analyzed by EDX. The presence of Zn, O and La elements were observed through EDX analyses and no other elements were detected in the spectra (Fig. 4a–c). This indicates that the prepared thin films are pure and free from impurities. A peak observed around 2 keV is attributed to Si (Si Kα) and which is exhibited from the glass substrates due to the depth of electron beam penetration. The EDX results are presented in Table 1 and it showed the difference in Zn/O and La/Zn ratio with the variation of La doping concentration. This is suggesting the oxygen deficiency of the films and the material with oxygen deficiency is highly suitable for gas sensor applications [32].

The growth mechanism of the resultant ZnO nanocorn morphology is still unclear but it was understood based on the experimentally observed results of pure and La: ZnO thin films and proposed (Fig. 5). The Zn^{2+} ions in the ZnO precursor solution were stabilized by diethanolamine (stabilizing agent) and make it crystal clear and homogeneous, which clearly indicates the interaction of diethanolamine in the ZnO precursor solution. In the first stage of deposition of ZnO thin film (Step 1), the cleaned glass substrate was immersed in the ZnO precursor solution with the controlled speed and thereby the adsorption of amine based $Zn(OH)_2$ complex is takes place over the glass substrate. Incessantly the glass substrate was dipped in DD water at 90 °C which is otherwise called an anionic solution and the intermediate $[Zn(OH)_4]^{2-}$ was formed on the substrate (Step 2). The water molecules (at 90 °C) removed the loosely bonded

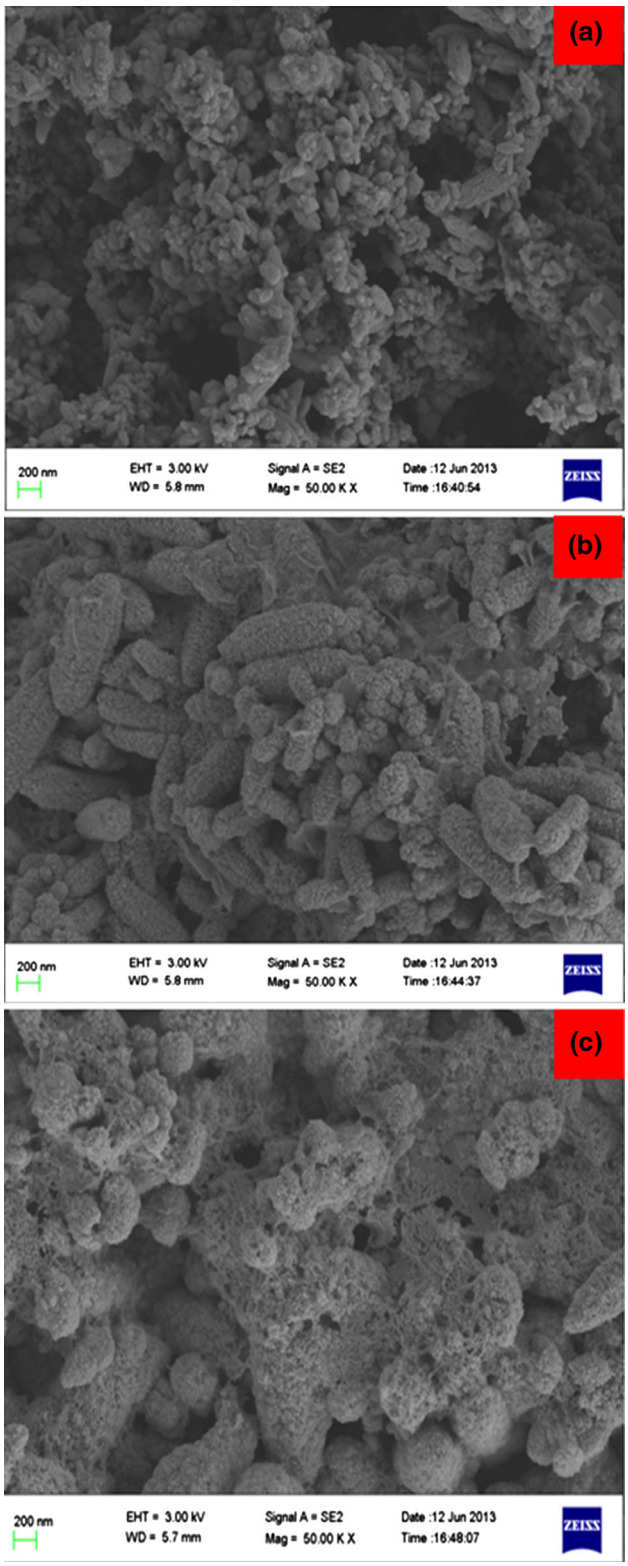

Fig. 3 FESEM images of **a** pure; **b** 5 wt%; **c** 10 wt% of La incorporated ZnO thin films

intermediate $[Zn(OH)_4]^{2-}$ molecules while withdrawing the substrate. Then the intermediate $[Zn(OH)_4]^{2-}$ molecules become to $Zn(OH)_2$ in the drying process at 100 °C

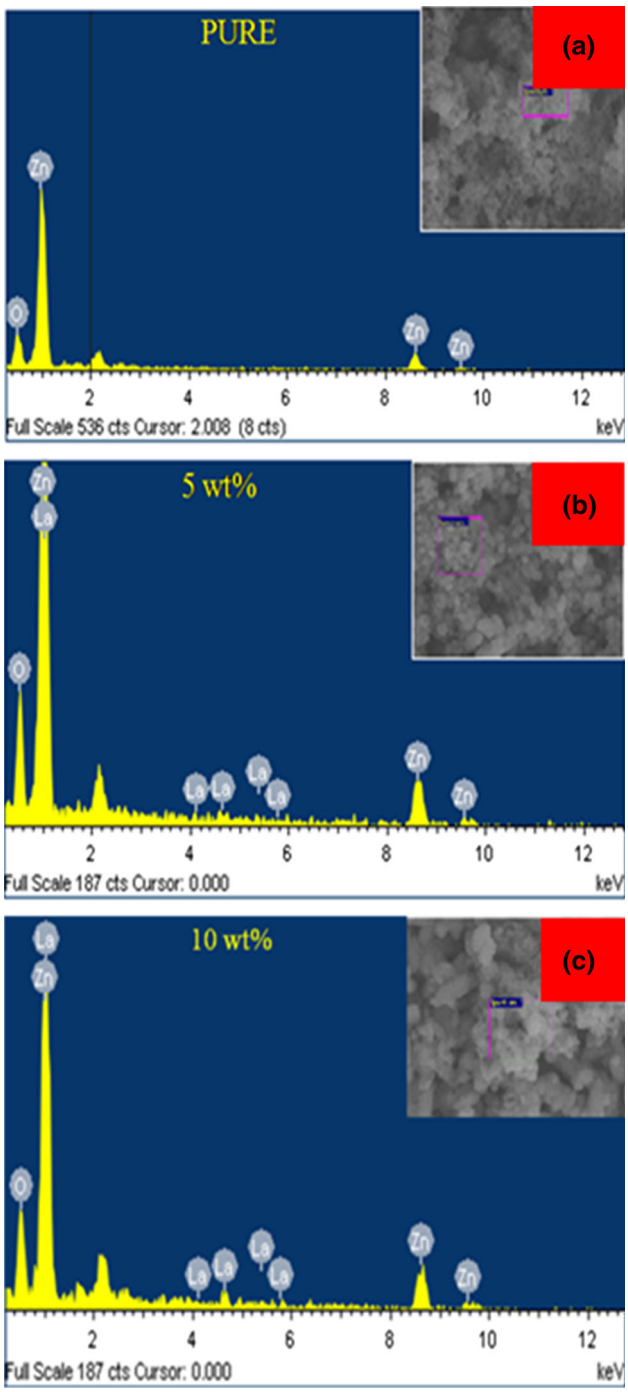

Fig. 4 EDX spectra of **a** pure; **b** 5 wt%; **c** 10 wt% of La incorporated ZnO thin films

Table 1 Elemental composition of pure and La: ZnO thin films

Elements	Pure ZnO	5 wt% of La incorporated ZnO	10 wt% of La incorporated ZnO
O	22.89	22.12	21.67
Zn	77.11	73.62	69.61
La	–	4.26	8.72

(Step 3). As shown in the Fig. 5, there are two types interaction may be possible between the $Zn(OH)_2$ and the amine group. They are (1) one oxygen atom from $Zn(OH)_2$ is attracted by one hydrogen atom from the DEA chain due to the ionic-dipolar interaction. Basically, DEA is a weak base which contains higher H^+ concentration due to its incomplete protonation and hence DEA chains attract with each other by the hydrogen bonding forces. Likewise, the ZnO nuclei [$Zn(OH)_2$] can grew with DEA chain due to the bonding of each DEA chains [33]. (2) A basic nitrogen atom of amine group contain a lone pair of electrons, which can interact with the Zn^{2+} ions of $Zn(OH)_2$ and thus ZnO nuclei can grew with DEA. During the annealing process at 350 °C, ZnO nuclei tend to become ZnO nanoparticles at a faster rate because of the removal of DEA chains, which causes the formation of corn morphology. The planes of ZnO namely (002), (110) and (101) have the lowest surface free energy of 9.9, 12.3 and 20.9 eV/nm^2 [34]. The incorporation of La on ZnO lattice enormously raises the stress in ZnO thin film which was further decreases the surface free energy of the film. Thus the stress in ZnO lattice upon La incorporation as well as the lowest surface free energy of the plane (002), favored the oriented attachment of ZnO nanoparticles along the (002) direction and thus the film became highly (002) textured.

In general, four photoluminescence (PL) emissions can be observed for ZnO. They are (1) ultraviolet emission otherwise near band edge emission (NBE) at around 390 nm and it is attributed to the exciton recombination (2) blue emission at around 460 nm is due to the intrinsic defects such as oxygen and zinc interstitials (3) green emission or deep level emission (DLE) at around 540 nm, which is probably arises from the electron–hole recombination caused by intrinsic point defects and surface defects such oxygen vacancies, zinc interstitials, incorporation of hydroxyl groups in ZnO lattice [35, 36].

Room temperature PL spectra of pure and La: ZnO thin films were recorded in the wavelength range from 350 to 600 nm with an excitation wavelength of 320 nm and it is shown in Fig. 6. A PL emission exhibited at 392 nm for pure ZnO is corresponds to the near band emission otherwise known as ultraviolet emission. This is generally ascribed to the recombination of free excitons. The strong photoluminescence intensity due to the La incorporation infers that La ions are playing as an effective luminescent centers and it is consistent with the previous report [37]. It is to be noticed that the increase in the intensity of the PL emission with the increase of La incorporation may be due to the c-axis oriented crystalline growth of ZnO upon La doping. At the same time it is interesting to note that the PL emission is slightly blue shifted from 392 (pure) to 388 nm (10 wt% of La: ZnO) and this may be ascribed to the particle size reduction. The blue shift may be attributed to

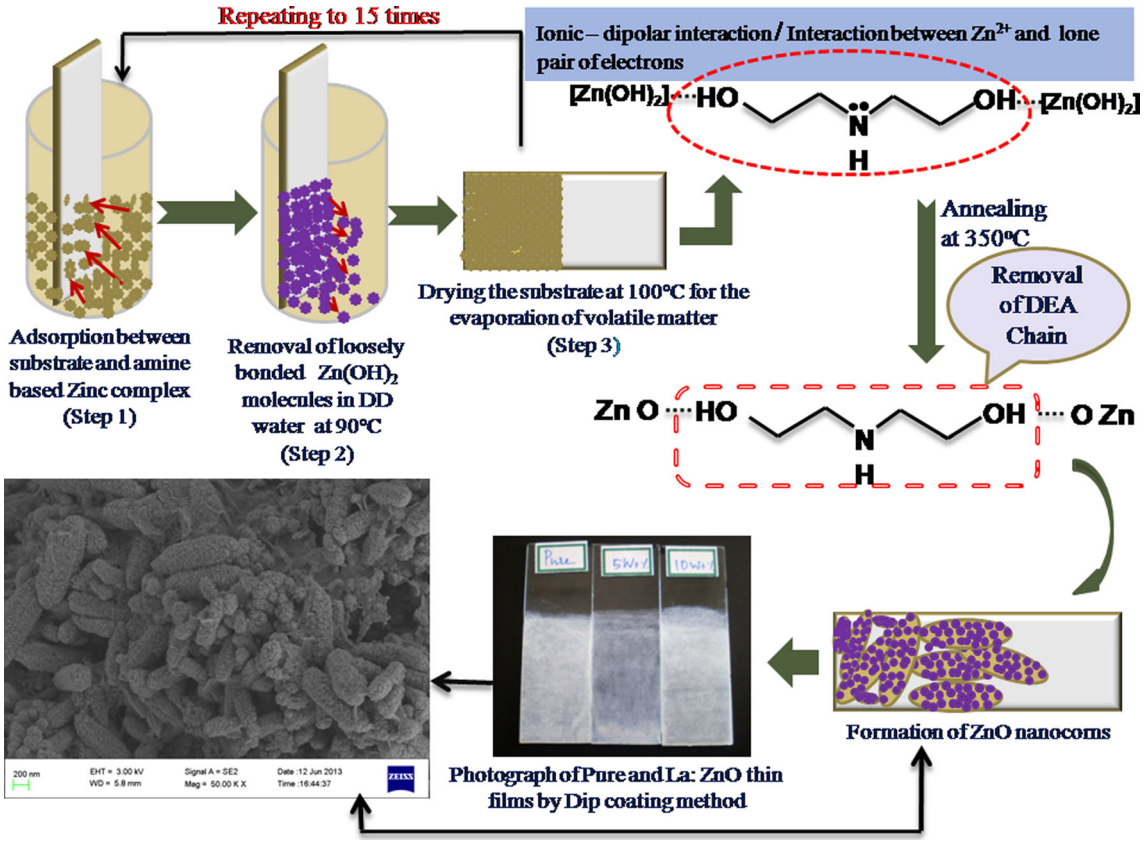

Fig. 5 Schematic illustration of the growth mechanism of ZnO nanocorns

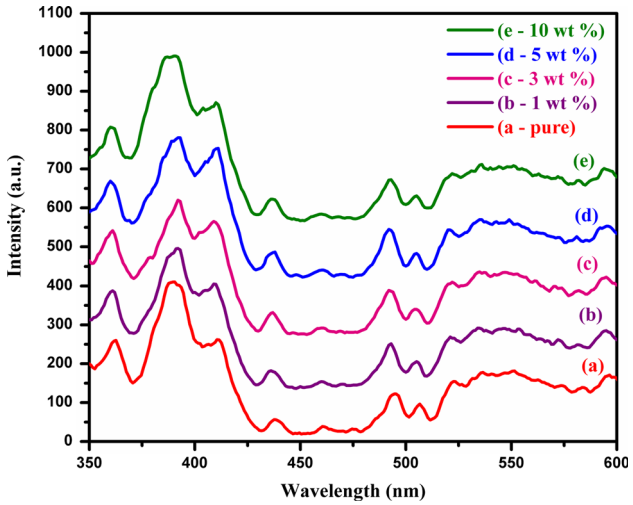

Fig. 6 Room temperature photoluminescence spectra of pure, 1, 3, 5 and 10 wt% (*a*–*e*) of La incorporated ZnO thin films

the ZnO lattice strain due to La incorporation [38]. The PL band at around 490 nm is observed for the blue emission which is attributed to the interstitial defects due to La^{3+} [39]. A broad green emission is exhibited at around 540 nm which is also attributed to interstitial defects and oxygen vacancies create some surface defects in ZnO thin films [36].

Generally, in the case of n-type semiconducting metal oxide gas sensors, the change of resistivity with and without expose of test gases was measured and thereafter the sensitivity was calculated. For ZnO based gas sensor, the changes of resistivity is mainly induced by the adsorption and desorption of oxygen molecules recognized by the surface of the grains. The chemisorbed oxygen molecules trap the electrons from the conduction band of ZnO and become oxygen ions (O_2^-, O^{2-}, O^-) and thereby it reduces the overall conductivity of the material. It can be explained as follows [40]:

$$O_2(\text{gas}) \leftrightarrow O_2(\text{ads}) \leftrightarrow O_2(\text{ads}) + e^- \leftrightarrow O_2^-(\text{ads}). \quad (3)$$

Upon the introduction of the reducing gases such as H_2, H_2S, C_2H_5OH, they readily react with the oxygen ions by liberating the trapped electrons back to the conduction band of ZnO accompanied by the decrease of the resistivity. So the resistivity changes or the sensitivity of ZnO thin films depends on the concentration of adsorbed oxygen molecules [41].

The variation of resistivity with respect to time for pure and La (1, 3, 5 and 10 wt%) incorporated ZnO thin films

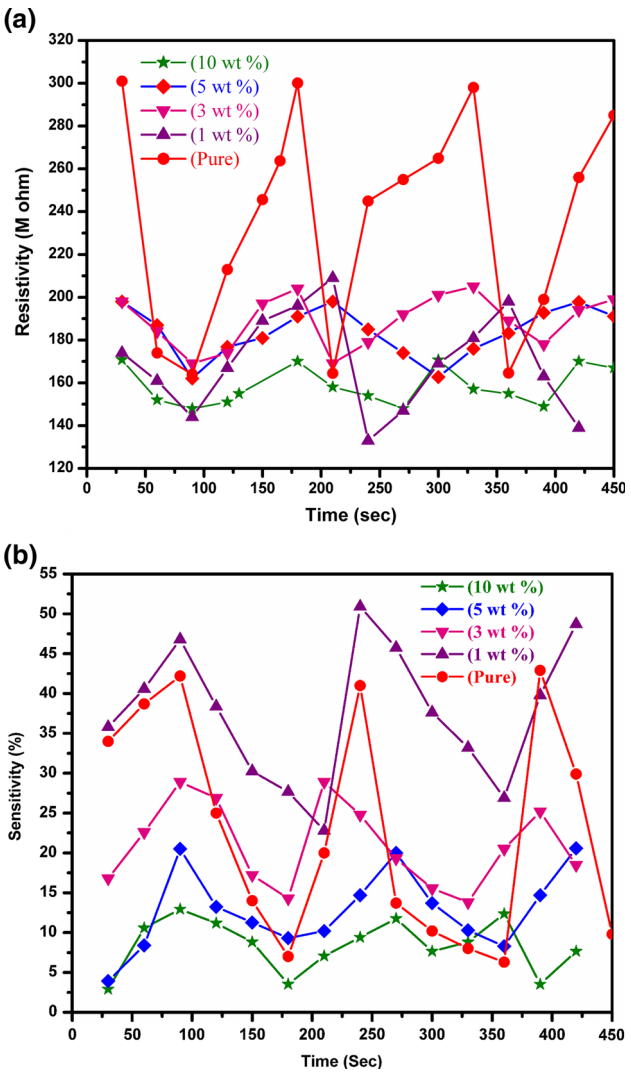

Fig. 7 **a** Resistivity of pure, 1, 3, 5 and 10 wt% of La incorporated ZnO thin films towards H_2 gas (1,000 ppm) at room temperature. **b** Sensitivity of pure, 1, 3, 5 and 10 wt% of La incorporated ZnO thin films towards H_2 gas (1,000 ppm) at room temperature

towards 1,000 ppm of H_2 gas concentration at room temperature was measured and presented in Fig. 7a. It is clearly observed that the resistivity of the pure ZnO thin film decreased upon exposing in the hydrogen gas, i.e. the chemisorbed oxygen molecules reacted with the hydrogen gas and producing H_2O molecules with releasing electrons. The electrons go to the conduction band of ZnO and thereby the resistivity of the film decreased. The resistivity is back to its original value, when the hydrogen supply was stopped. Subsequently the resulted water desorbs quickly due to the exothermic nature of the reaction [42]. This sensing mechanism can be written as follows [43]:

$$O^-_{ads} + H_2 \rightarrow H_2O + e^-. \quad (4)$$

The resistivity of the ZnO thin film in air drastically decreased with the increase of La incorporation, because a trivalent lanthanum acts as a donor to ZnO, thereby the electrical resistivity of La: ZnO films compared to pure ZnO film was decreased. The sensitivity (S) of the pure ZnO, 1, 3, 5 and 10 wt% of La incorporated ZnO thin films were observed to be 43, 51, 29, 21 and 13 respectively (Fig. 7b) at room temperature.

It is clearly observed that 1 wt% of La incorporated ZnO thin film showed high sensitivity (51) at room temperature. At this lower concentration of La, the carrier concentration of physisorbed oxygen molecules (O_2^-, O^{2-}, O^-) is higher than the pure ZnO, which leads to the drastic change in resistivity upon H_2 gas exposure. Hence, the sensitivity is observed to be higher than the pure ZnO. The H_2 gas sensitivity of 3, 5 and 10 wt% of La: ZnO thin films are observed to be decrease than pure ZnO. The decrease in the sensitivity (S) associated with the higher concentration of (3, 5 and 10 wt%) of La: ZnO thin films are due to the congregation of Lanthanum oxide phases over the surface of the ZnO and they could reduce the available active adsorption sites. Because, La^{3+} cannot enter in the ZnO lattice (Ionic radii of Zn^{2+}: 0.074 nm, La^{3+}: 0.106 nm and O^{2-}: 0.132 nm). Though, there is an oxygen deficiency in the La: ZnO films (in accordance with the EDX results), La based superfluous over the sensing layer affect the sensitivity because the sensing mechanism is based on the surface reaction only. So the decrease of the sensitivity for higher concentration (3, 5 and 10 wt%) of La: ZnO thin films may be ascribed to the superfluous of the La on the grain boundaries of ZnO [40].

4 Conclusion

Pure and La incorporated ZnO thin films with novel corn like morphology were successfully prepared on glass substrates by a cost effective sol–gel dip coating method. TGA/DTA analysis suggested the formation of ZnO at around 350 °C. XRD analysis confirmed the presence of ZnO with hexagonal structure and also it emphasized that La incorporation induce the growth of ZnO thin films along c-axis with the preferred orientation of (002) plane. FESEM images demonstrated that the prepared thin films showed novel corn like morphology composed by the well defined spherical nanoparticles and moreover it ascertained the elongation of nanocorns along c-axis upon La incorporation. La: ZnO thin films exhibited an enhanced PL intensity, which infers that La increases photoluminescence property. 1 wt% of La incorporated ZnO thin film showed good sensitivity (S = 51 %) for H_2 gas at room temperature. The sensing performance of La: ZnO thin films (3, 5, 10 wt%) were found to decrease compared to the pure ZnO due to the superfluous of La on the grain boundaries of ZnO. Finally, it is concluded that higher concentration of the La incorporation in ZnO thin films decreases the H_2 gas sensitivity.

Acknowledgments The work was financially assisted by University Grants Commission through the scheme of UGC Major Research Project (No. F. 40-74/2011 (SR) and highly acknowledged. The authors are also grateful to thank School of Physics, Alagappa University, Karaikudi for extending XRD and PL facility to carry out the work.

References

1. H. Gu, Z. Wang, Y. Hu, Hydrogen gas sensors based on semiconductor oxide nanostructures. Sensors **12**, 5517–5550 (2012)
2. T. Hubert, L. Boon Brett, G. Black, U. Banach, Hydrogen sensors—a review. Sens. Actuators B **157**, 329–352 (2011)
3. W.J. Buttner, M.B. Post, R. Burgess, C. Rivkin, An overview of hydrogen safety sensors and requirements. Int. J. Hydrog. Energy **36**, 2462–2470 (2011)
4. M. Aroutiounian, Hydrogen detectors. Int. Sci. J. Altern. Energy Ecol. **3**, 21–31 (2005)
5. N.L. Hung, E. Ahn, S. Park, H. Jung, H. Kim, S.K. Hong, D. Kim, C. Hwang, Synthesis and hydrogen gas sensing properties of ZnO wire like thin films. J. Vac. Sci. Technol. A **27**, 1347–1351 (2009)
6. N.H. Al-Hardan, M.J. Abdullah, A.A. Aziz, Sensing mechanism of hydrogen gas sensors based on RF sputtered ZnO thin films. Int. J. Hydrog. Energy **35**, 4428–4434 (2010)
7. C.D. Lokhande, P.M. Gondkar, S.M. Rajaram, V.R. Shinde, S.H. Han, CBD grown ZnO based gas sensors and dye sensitized solar cells. J. Alloys Compd. **475**, 304–311 (2009)
8. H.A. Khorami, A. Eghbali, M.K. Rad, M.R. Vaezi, M. Kazemzad, Ammonia sensing properties of (SnO_2-ZnO)/polypyrrole coaxial nanocables. J. Mater. Res. **49**, 685–690 (2014)
9. W. Guo, T. Liu, Z. Gou, W. Zeng, Y. Chen, Z.C. Wang, Hydrothermal synthesis of ultrathin ZnO nanosheets and their gas sensing properties. J. Mater. Sci. Mater. Electron. (2012). doi:10.1007/s10854-012-1009-x
10. C. Jayaseelan, A.A. Rahuman et al., Novel microbial route to synthesize ZnO nanoparticles using *Aeromonas hydrophila* and their activity against bacteria and fungi. Spectrochim. Acta A **90**, 78–84 (2012)
11. Q. Yuan, S. Hein, R.D.K. Misra, New generation of chitosan encapsulated ZnO quantum dots loaded with drug; synthesis, characterization and in vitro drug delivery response. Acta Biomater. **6**, 2732–2739 (2010)
12. K. Vijayalakshmi, K. Karthick, K. Tamilarasan, Enhanced H2 sensing properties of a-plane ZnO prepared on c-cut sapphire substrate by sputtering. J. Mater. Sci. Mater. Electron. **24**, 1325–1331 (2013)
13. V. Vasanthipillay, K. Vijayalakshmi, Effect of power on the structural properties of indium tin oxide thin film prepared for application in hydrogen gas sensor. J. Mater. Sci. Mater. Electron. **24**, 1895–1899 (2013)
14. S.K. Arya, S. Krishnan, H. Silva, S. Jean, S. Bhansali, Advances in materials in room temperature hydrogen gas sensors. Analyst **137**, 2743–2756 (2012)
15. S.B. Patil, A.K. Singh, Solution grown nanocrystalline ZnO thin films for UV emission and LPG sensing. J. Mater. Sci. **45**, 5204–5210 (2010)
16. T. Minami, New n-type transparent conducting oxides. Mater. Res. Bull. **25**, 38–44 (2000)
17. S.S. Badadhe, I.S. Mulla, Effect of aluminium doping on structural and gas sensing properties of Zinc oxide thin films deposited by spray pyrolysis. Sens. Actuators B **156**, 943–948 (2011)
18. S.D. Gopal Ram, M. Anbu Kulandainathan, G. Ravi, On the study of pH effects in the microwave enhanced rapid synthesis of nano ZnO. Appl. Phys. A **99**, 197–203 (2010)
19. D. Guo, K. Sato, S. Hibino, T. Takeuchi, H. Bessho, K. Kazumi, Low-temperature preparation of transparent conductive Al-doped ZnO thin films by a novel sol–gel method. J. Mater. Sci. (2014). doi:10.1007/s10853-014-8172-9
20. K.S. Venkatesh, N.S. Palani, S.R. Krishnamoorthi, V. Thirumal, R. Ilangovan, Fungus mediated biosynthesis and characterization of zinc oxide nanorods. AIP Conf. Proc. **1536**, 93–94 (2013)
21. R.Y. Hong, J.H. Li, L.L. Chen, D.Q. Liu, H.Z. Li, Synthesis, surface modification and photocatalytic property of ZnO nanoparticles. Powder Technol. **189**, 426–432 (2009)
22. X. Niu, W. Du, W. Du, Preparation, characterization and gas sensing properties of rare earth mixed oxides. Sens. Actuators B **99**, 399–404 (2004)
23. B.L. Zhu, C.S. Xie, A.H. Wang, D.W. Zeng, M.L. Hu, W.Y. Wang, Electrical conductivity and gas sensitivity of Zn–Sb–O thick films. Mater. Res. Bull. **39**, 409–415 (2004)
24. D.S. Lee, K.H. Nam, D.D. Lee, Effect of substrate on NO_2 sensing properties WO_3 thin film gas sensors. Thin Solid Films **375**, 142–146 (2000)
25. K. Sivakumar, V. Senthilkumar, N. Muthukumarasamy, M. Thambidurai, T.S. Senthil, Influence of pH on ZnO nanocrystalline thin films prepared by sol–gel dip coating method. Bull. Mater. Sci. **35**, 327–331 (2012)
26. H. Bahadur, S.B. Samanta, A.K. Srivastava, K.N. Sood, R. Kishore, R.K. Sharma, A. Basu, Rashmi, M. Kar, P. Pal, V. Bhatt, S. Chandra, Nano and micro structural studies of thin films of ZnO. J. Mater. Sci. **41**, 7562–7570 (2006)
27. C.Z. Wang, D. Xu, X. Xiao, Y. Zhang, D. Zhang, Effects of oxygen pressure on the structural and photoluminescence of ZnO thin films. J. Mater. Sci. **42**, 9795–9800 (2007)
28. K. Vijayalakshmi, K. Karthick, P. Deepak Raj, M. Sridharan, Influence of thickness of MgO overlayer on the properties of ZnO thin films prepared on c-plane sapphire for H_2 sensing. Ceram. Int. **40**, 827–833 (2014)
29. S.K. Gupta, A. Joshi, M. Kaur, Development of gas sensors using ZnO nanostructures. J. Chem. Sci. **122**, 57–62 (2010)
30. W. Lan, Y. Liu, M. Zhang, B. Wang, H. Yan, Y. Wang, Structural and optical properties of La-doped ZnO films prepared by magnetron sputtering. Mater. Lett. **61**, 2262–2265 (2007)
31. S. Mondal, S.R. Bhattacharyya, P. Mitra, Preparation of manganese doped-ZnO thin films and their characterization. Bull. Mater. Sci. **36**, 223–229 (2013)
32. C. Balamurugan, A. Subhashini, G.N. Chaudhari, A. Subramania, Development of wide band gap sensor based on $AlNbO_4$ nanopowder for ethanol. J. Alloys Compd. **526**, 110–115 (2012)
33. R. Razali, A.K. Zak, W.H.Abd. Majid, M. Darroudi, Solvothermal synthesis of microsphere ZnO nanostructures in DEA media. Ceram. Int. **37**, 3657–3663 (2011)
34. Y. Bouznit, Y. Beggah, F. Ynineb, Sprayed lanthanum doped Zinc oxide thin films. Appl. Surf. Sci. **258**, 2967–2971 (2012)
35. D.R. Patil, L.A. Patil, D.P. Amalnerkar, Ethanol gas sensing properties of Al_2O_3-doped ZnO thick film resistors. Bull. Mater. Sci. **30**, 553–559 (2007)
36. S. Xu, Z.L. Wang, One-dimensional ZnO nanostructures: solution growth and functional properties. Nano Res. **4**, 1013–1098 (2011)
37. A. Ghosh, N.G. Deshpande, Y.G. Gudage, R.A. Joshi, A.A. Sagade, D.M. Phase, R. Sharma, Effect of annealing on structural and optical properties of zinc oxide thin film deposited by successive ionic layer adsorption and reaction technique. J. Alloys Compd. **469**, 56–60 (2009)
38. D. Sridevi, K.V. Rajendran, Enhanced optical properties La doped ZnO nanoparticles. Optoelectron. Adv. Mater. Rapid Commun. **4**, 1591–1593 (2010)
39. L.A. Jose, J.M. Linet, V. Sivasubramanian, A.K. Arora, C.J. Raj, T. Maiyalagan, S.J. Das, Optical properties of nano-structured

La-doped ZnO prepared by combustion method. Mater. Sci. Semicond. Process. **15**, 308–313 (2012)
40. A.K. Singh, V. Viswanath, V.C. Janu, Synthesis, effect of capping agents, structural, optical and photoluminescence properties of ZnO nanoparticles. J. Lumin. **129**, 874–878 (2009)
41. O. Lupan, G. Chai, L. Chow, Novel hydrogen gas sensor based on single ZnO nanorods. Microelectron. Eng. **85**, 2220–2225 (2008)
42. C. Ge, C. Xie, S. Cai, Preparation and gas-sensing properties of Ce-doped ZnO thin-film sensors by dip-coating. Mater. Sci. Eng. B **137**, 53–58 (2007)
43. S. Saito, M. Miyayama, K. Kuomoto, H. Yanagida, Gas sensing characteristics of porous ZnO and Pt/ZnO ceramics. J. Am. Ceram. Soc. **68**, 40–43 (1985)

Indian J Phys
DOI 10.1007/s12648-014-0601-8

ORIGINAL PAPER

Facile one step synthesis of novel TiO_2 nanocoral by sol–gel method using *Aloe vera* plant extract

K S Venkatesh[1], S R Krishnamoorthi[1], N S Palani[1], V Thirumal[1], S P Jose[2], F-M Wang[3] and R Ilangovan[1]*

[1]Nanoelectronics Laboratory, Department of Nanoscience and Technology, Alagappa University, Karaikudi 630 004, Tamil Nadu, India

[2]School of Physics, Madurai Kamaraj University, Madurai 625 021, Tamil Nadu, India

[3]Graduate Institute of Applied Science and Technology, National Taiwan University of Science and Technology, 43 Keelung Road, Section 4, Taipei 106, Taiwan

Received: 17 June 2014 / Accepted: 08 September 2014

Abstract: Titanium oxide (TiO_2) nanoparticles (NPs) were synthesized by sol gel method using *Aloe vera* plant extract as a biological capping agent and a cauliflower-nanocoral morphology was observed in this technique. The assynthesized TiO_2 nanopowder was calcined at a range of temperatures (300–600 °C) for 1 h. The influence of *A. vera* plant extract on the thermal, structural and morphological properties of TiO_2 nanopowder was evaluated. Thermogravimetric analysis/differential thermal analysis was employed to study the thermal properties of the assynthesized TiO_2 nanopowder. The crystallinity, phase transformation and the crystallite size of the calcined samples were studied by X-ray diffraction technique. XRD result confirmed the presence of TiO_2 with anatase phase. FT Raman spectra showed the Raman active modes pertaining to the TiO_2 anatase phase and Raman band shift was also observed with respect to particle size variation. The different functional group vibrations of as dried pure *A. vera* plant extract were compared with the mixture of TiO_2 and *A. vera* plant extract by FT-IR analysis. The scanning electron microscopy images apparently showed the formation of spherical shaped NPs and also it demonstrated the effect of *A. vera* plant extract on the reduction of particles size. The surface area of the TiO_2 NPs was measured through Brunauer–Emmett–Teller analysis. Transmission electron microscopy images ascertained that the spherical shaped TiO_2 NPs were formed with cauliflower-nanocoral morphology decorated with nanopolyps with the size range between 15 and 30 nm.

Keywords: *Aloe vera*; TiO_2 nanocorals; X-ray diffraction; Raman spectroscopy; Electron microscopy

PACS Nos.: 81.16.Ta; 77.84.Bw; 61.05.cp; 78.30.Am; 78.30.Fs; 68.37.Hk; 68.37.Lp

1. Introduction

In the past few decades, nanomaterials are highly attracted by researchers to exploit their excellent properties for various applications. Among the semiconductor metal oxides, TiO_2 is a fascinating and one of the technologically important materials in the field of nanotechnology and it governs the keen interest of scientific community, due to its salient properties such as high chemical stability, wide band gap, good mechanical resistance and high optical transmittance in visible and IR spectral range [1]. TiO_2 exists in three polymorphs: rutile (Tetragonal), anatase (Tetragonal) and brookite (Orthorhombic). One dimensional TiO_2 nanowire structure has the potential application in dye sensitized solar cells (DSSCs) [2–6] and also TiO_2 is being greatly used in many applications such as photo catalysts [7, 8], gas sensors [9], electro chromic devices [10], antibacterial activity [11] and it also finds applications in biomedical sciences such as bone, tissue engineering and in pharmaceutical industries due to its non toxicity [12] and so on. TiO_2 nanoparticles (NPs) with different nanostructures have been synthesized by electrospinning method [13], hydrothermal method [14, 15], template method [16] etc.

Aloe barbadensis miller is one of the important medicinal plants and also it is known as the "Lily of the Desert". The raw pulp of *Aloe vera* contains approximately 0.5 % solid material consists of a variety of compounds including

*Corresponding author, E-mail: rajangamilangovan@gmail.com

Published online: 12 October 2014

water soluble and fat soluble vitamins, minerals, enzymes, polysaccharides, phenolic compounds, organic acids and remaining 99.5 % are water [17–19].

Synthesis of gold nano triangles and silver NPs using *A. vera* plant extract as reducing agent has been reported [20, 21]. Moreover, *A. vera* plant extract has been used to synthesize metal oxide NPs such as ZnO [22, 23], CuO [24], MFe_2O_4 (where M = Cu, Ni and Zn) NPs [25], hydroxyapatite (HAp) powders [26], In_2O_3 [27] and microorganisms have also been reported for the synthesis of metal oxides [28]. NPs synthesized by chemical methods are involved with toxic chemicals and adsorbed on its surface, which causes adverse effect in the medical applications. Synthesis of NPs using bio-capping agents offer non toxic, facile and one step synthesis with easiest protocol, sustainable and easy scale up to the industrial production at lower cost. Moreover, the uses of environmentally benign materials for the synthesis of NPs offer eco-friendliness and compatibility for pharmaceutical and biomedical applications as they do not use toxic chemical for the synthesis protocol [24]. Synthesis of different nanostructures is gaining a great importance in both fundamental scientific research and technological applications owing to their interesting physico-chemical properties. A nanocoral is one of the novel architecture and it has potential application in DSSCs. Synthesis of TiO_2 nanocorals is highly difficult and it has been achieved by means of multi step hydrothermal process [29], polymer gel templating procedure [30] etc. These methods involve multistep processes, time, power consuming, toxic chemicals and expensiveness and so on.

Sol–gel method is one of the best methods for the preparation of metal oxides. It offers an easy synthesis procedure to achieve nano scale counterparts by controlling the synthesis conditions. This method provides many advantages and to name a few are room temperature synthesis under atmospheric pressure, purity, homogeneity, to introduce desire amount of dopants, stoichiometry control and financially viable. However, it is very difficult to individually control the three reactions such as hydrolysis, condensation and agglomeration, which occurs simultaneously in sol–gel process. So, a slight change in experimental condition modifies the particle size and morphology [31, 32]. A fresh *A. vera* plant extract contains many biologically active components, such as polysaccharides vitamins, proteins, lipids, polyphenols, heterocyclic and carbonyl compounds and so on. In the extracellular synthesis of NPs using plants, on one hand, some biomolecules can act as reducing agent, on the other hand, some biological constituents can act as capping agent for the resulting NPs. As a result, the aggregation of resulting NPs could be impeded by means of stabilization due to the protein- nanoparticle interaction and also the surface morphology can be influenced by the shape-directing ability of the carbonyl compound present in the *A. vera* plant extract. Hence, it is anticipated that this synergistic effect of *A. vera* plant extract (both stabilization and capping) might influence on the morphology and size of TiO_2.

In this communication, the facile one step sol–gel synthesis of novel TiO_2 nanocoral architecture using *A. vera* plant extract as a bio-capping agent is reported. It has been clearly observed that *A. vera* plant extract proves its efficacy on the thermal, structural and morphological properties of TiO_2 NPs as expected. A novel TiO_2 nanocoral architecture through simple experimental procedure such as sol gel method using *A. vera* plant extract as bio-capping agent is demonstrated.

2. Experimental details

Titanium isopropoxide (SD Fine Chemicals), Ethanol, absolute (MERCK) and *A. vera* plant extract were used as starting materials for the preparation of pure and *A. vera* capped TiO_2 precursor solution. Fresh and matured leaves of *A. vera* plant were harvested from the local agricultural land. Then, 30 g of thoroughly washed *A. vera* leaves were finely cut and boiled in 100 ml of deionized water. The resulting extract was used for further experiments [20]. Pure TiO_2 precursor solution was prepared by drop wise addition of 3 ml of Titanium isopropoxide in 20 ml of ethanol under magnetic stirring. Similarly, *A. vera* capped TiO_2 precursor solution was prepared by adding 0.5, 0.75 and 1 ml of *A. vera* plant extract during the preparation of pure TiO_2 precursor solution and they were coded as 1AT, 2AT and 3AT respectively. After 3 h under continuous stirring, the pure and *A. vera* capped TiO_2 precursor solutions were subjected to heating (100 °C) under stirring, until the xerogel completely dried and finally cooled to room temperature. By adding titanium isopropoxide in ethanol solution, $Ti(OH)_4$ was formed. Upon subsequent heating at 100 °C, the formation of TiO_2 took place due to the condensation process. The relevant chemical reaction process were followed, as given in Eqs. (1a) and (1b).

$$\mathrm{Ti}\{\mathrm{OCH(CH_3)_2}\}_4 + 4\mathrm{C_2H_5OH} \longrightarrow \mathrm{Ti(OH)_4} + 4\mathrm{(CH_3)_2}\underset{|}{\mathrm{CH}}\mathrm{-O-C_2H_5} \quad (1a)$$

$$\mathrm{Ti(OH)_4} \xrightarrow{\Delta(100\ ^\circ\mathrm{C})} \mathrm{TiO_2} + 2\mathrm{H_2O} \quad (1b)$$

The dried precursor was crushed into fine powder using agate mortar and pestle. Finally, the grinded powder was calcined at different temperatures in a tubular furnace (Carbolite, UK) in an ambient atmosphere. Before calcination, the thermal behavior of the as-synthesized TiO_2 powder was analyzed by means of Thermo Gravimetric and Differential Thermal Analysis (EXSTAR

6000 TG/DTA) from ambient to 900 °C with the heating rate of 10 °C/min in air atmosphere. XRD pattern was recorded by Cu Kα radiation (1.54060 Å) using PANalytical X-PERT PRO diffractometer system. The morphology was examined by scanning electron microscopy (SEM) (Model: Hitachi S3000 H SEM). The surface area was measured by Brunauer–Emmett–Teller (BET) using MICROMETRICS ASAP 2020 POROSIMETER. FT- Raman spectra were obtained by BRUKER RFS 27 FT-Raman spectrometer. The functional group vibrations of the 2AT and the pure *A. vera* plant extract powders were analyzed by FTIR analysis (Model: Perkin Elmer Spectrum RX I). Transmission Electron Microscopy (Model: JEOL-200 FXII) was employed to confirm the nanocoral structure and also to measure the size of the NPs.

3. Results and discussion

In the preparation of TiO_2 precursor solution, it has been observed that the precursor solution is clear even after the addition of titanium isopropoxide with the ethanol solution, which manifests the complete dissolution of the metal alkoxide in the solvent. This clear solution immediately becomes to slurry with pale green colour followed by the addition of *A. vera* plant extract and it has been happened due to the rapid reaction of the precursor solution through hydrolysis and condensation caused by the presence of water molecules in *A. vera* plant extract. The colour change indicates the encapsulation of TiO_2 particles by small amount of solid biomolecules (0.5–1 %) contain in the *A. vera* plant extract and also the pale green colour becomes rich with respect to the increase of *A. vera* plant extract. The colour of the as-synthesized powder has been changed to pure white, after the calcination process which implies the elimination of biomolecules from the powder.

The TGA/DTA analysis has been performed for the as-synthesized (1AT and 3AT) TiO_2 nanopowder. In TGA curve of 1AT sample, the weight loss around 100 °C is attributed to the removal of physically and chemically entrapped water and a further weight loss at 210 °C is attributed to the elimination of organic matrix, as shown in Fig. 1(a). There is no further weight loss after 300 °C and in association with DTA curve, the oxidation process of the powder is initiated at the same temperature (300 °C), which indicates the formation of metal oxide. In the case of 3AT sample, physically and chemically entrapped water removed at 100 °C and the removal of organic matrix takes place around 235 °C, as shown in Fig. 1(b). This small increase in temperature for 3AT is due to the presence of more surface energy offered by the NPs compared to the 1AT sample. Hence it is understood that biological

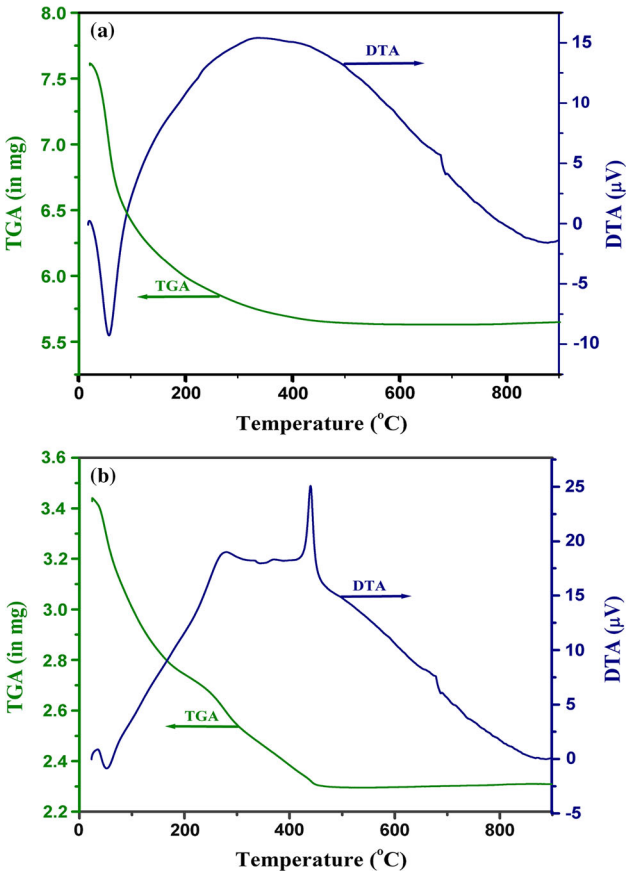

Fig. 1 TGA/DTA curve of as-synthesized TiO_2 nanopowder. (**a**) 1AT and (**b**) 3AT

molecules enter in the metal oxide matrix and serve as capping agent. In DTA curve (3AT) a small exothermic region around 300 °C indicates the crystallization of the TiO_2 nanopowder followed by the oxidation process. In TGA curve, the further weight loss is observed till 420 °C associated with the strong exothermic peak in DTA curve, which is due to complete removal of the sheath of biomass present over the NPs. In both cases, a small change observed at around 670 °C may be attributed to the phase transformation of TiO_2 from anatase to rutile.

As shown in the XRD pattern of 1AT and 2AT samples, the as-synthesized TiO_2 nanopowder is amorphous. After the calcination, the predominant peak found out for the 1AT, 2AT and 3AT samples at 25.3° (2θ) with (101) plane and other planes such as (004), (200), (211), (204), (116), (103), (112), (113), (105) are corresponding to anatase phase as shown in Fig. 2(a)–2(c). In the case of 1AT, the rutile phase of TiO_2 is also observed only at the calcination temperature of 600 °C and the planes (110), (101), (111), (210), (211), (220), (310) refers to the rutile phase, as shown in Fig. 2(a). All the observed diffraction peak values are closely match with the standard diffraction data (JCPDS File No: 89-4921, 89-4920). The crystallization

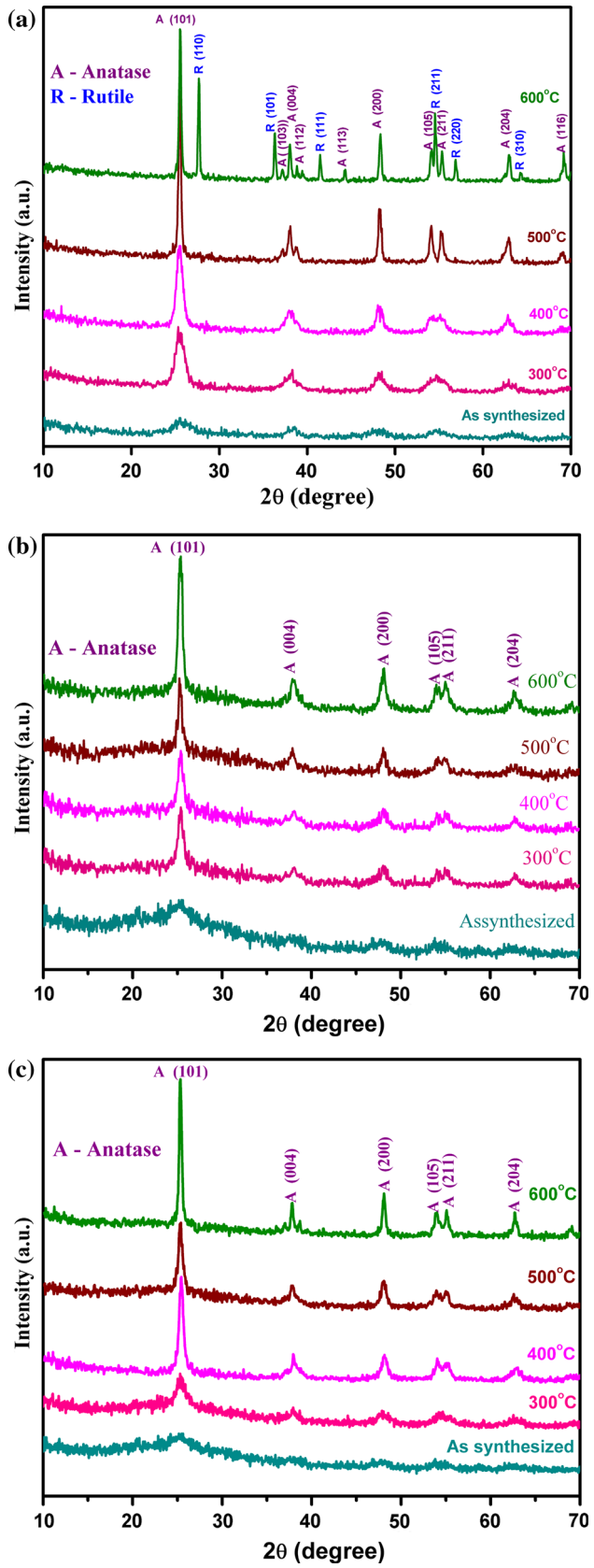

Fig. 2 XRD patterns of TiO_2 nanopowder. (**a**) 1AT, (**b**) 2AT and (**c**) 3AT

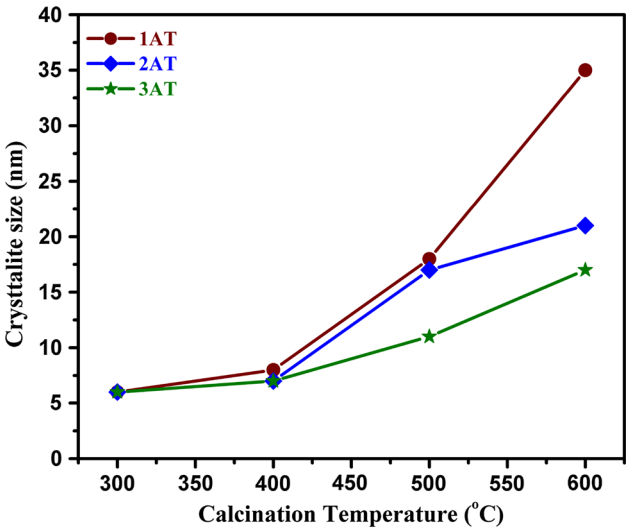

Fig. 3 Crystallite size versus calcination temperature of TiO_2 nanopowder

temperature of as-synthesized TiO_2 nanopowder has been observed at 300 °C for 1AT and 3AT samples and this is consistent with the TGA/DTA results. The free energy of rutile phase is always less than that of anatase phase, making the rutile is more stable phase at all temperatures. But the rutile phase has been not observed for 2AT and 3AT even at higher calcination temperature (600 °C) owing to higher concentration (0.75, 1 ml) of *A. vera* plant extract. The *A. vera* plant extract (0.75 onwards), which hinders the grain growth, thereby leads to the NPs and also retards the phase transformation. Hence, the phase transformation of TiO_2 from anatase to rutile can be controlled by bio-capping agent. Indeed, the improvement in the degree of crystallinity has been clearly observed with the increase of calcination temperature.

The crystallite size of the synthesized TiO_2 nanopowder has been calculated using scherrer equation (Eq. 2).

$$D = \frac{0.9\lambda}{\beta \cos\theta} \tag{2}$$

$$\frac{1}{d^2} = \frac{h^2 + k^2}{a^2} + \frac{l^2}{c} \tag{3}$$

where 0.9 is a constant, λ is the wavelength of X-ray source, β is the full width at the half maximum in radians, θ is the Bragg's diffraction angle. The effect of concentration of *A. vera* plant extract and the calcination temperature on the crystallite size of the synthesized TiO_2 nanopowder is presented in Fig. 3. The lattice constants are calculated using X ray diffraction data from the formula of Tetragonal crystal system (Eq. 3). The calculated lattice constants are presented in Table 1. These values are in close agreement with the standard values of both anatase and rutile phases

Table 1 Lattice constants of TiO_2 nanopowder

Sl. no.	Crystal system (tetragonal)	Standard values		Calculated values	
		a = b (Å)	c (Å)	a = b (Å)	c (Å)
1	Anatase	3.777	9.501	3.7856	9.5229
2	Rutile	4.584	2.953	4.5579	2.9524

Lattice constants of TiO_2 nanopowder

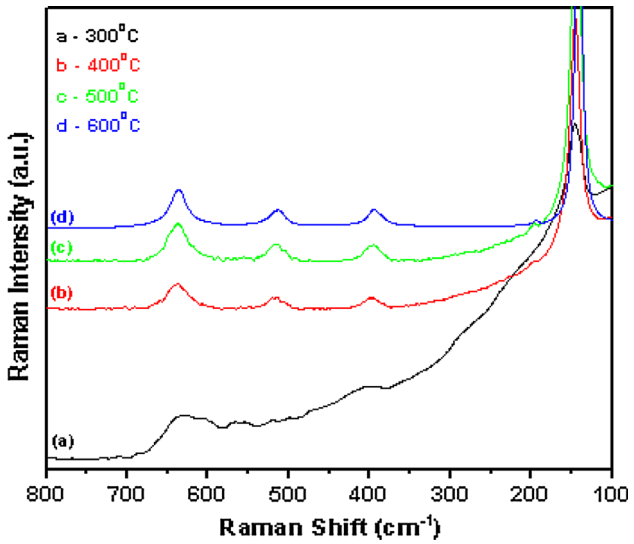

Fig. 4 FT Raman spectra of TiO_2 nanopowder (3AT)

of TiO_2. A small deviation in both phases of calculated lattice constant values with respect to those standard values may be due to the strain of the TiO_2 nanopowder caused by the heat treatment (calcination) and/or may be due to the instrumental error.

It is well known that TiO_2 exists in three polymorphs namely anatase, rutile and brookite. Rutile is thermodynamically stable, whereas anatase and brookite undergo irreversible exothermic transformation to rutile with respect to the range of temperature. Rutile, anatase and brookite phases of TiO_2 have 4, 6 and 36 Raman active modes, respectively [33, 34]. Figure 4(a)–4(c) show the FT- Raman spectra of TiO_2 nanopowder (3AT) calcined at 400 °C for 1 h. The appearance of strongest E_g mode at 144 cm^{-1} is due to the Ti–O streaching vibration bond which ascertains the presence of anatase phase in the TiO_2 nanopowder. The modes located at 144 (E_g), 197 cm^{-1} (E_g), 396.9 (B_{1g}), 515 (A_{1g}) and also 637 cm^{-1}(E_g) are responsible for the Raman active modes of anatase phase TiO_2 [35] and no other peaks have been detected, which indicates that the TiO_2 nanopowder posses anatase phase only. By comparing these spectra, it seems to be clear that the Raman bands are slightly shifted towards the higher wave number with respect to the increase of calcination

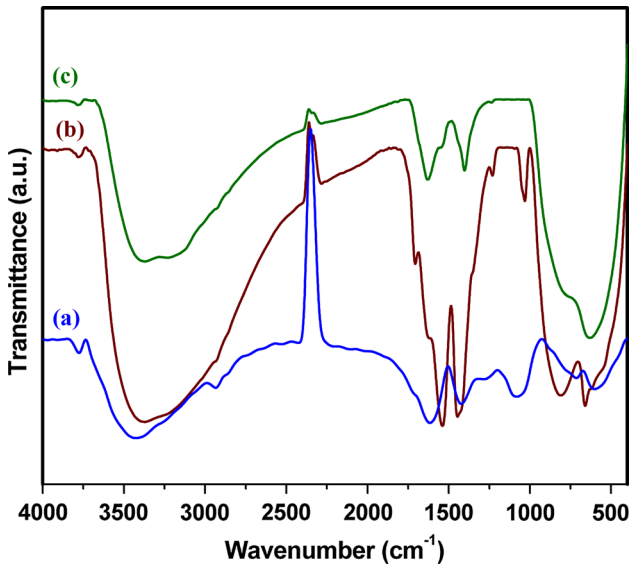

Fig. 5 FTIR spectra of *a* dried *Aloe vera* plant extract, *b* as synthesized TiO_2 nanopowder, *c* TiO_2 nanopowder calcined at 300 °C

temperature, which emphasizes the increase of the particle size. Also the increase of peak intensity with the increase of calcination temperature indicates the increase of crystallinity. There is no any Raman modes pertaining to the rutile phase and it suggested the absence of rutile phase and this result is consistent with the XRD results.

FTIR spectra of *A. vera* plant extract and TiO_2 nanoparticle are shown in Fig. 5(a)–5(c). A broad band at 3,423 cm^{-1} is assigned to hydrogen bonded –OH stretching vibration. A band observed at 1,615 cm^{-1} is attributed to the amide group vibration, which is a characteristic peak of proteins/enzymes [36]. The bands appeared at 1,421 and 1,080 are associated with carboxylic acid, C–N stretching vibration of amine group respectively, as shown in Fig. 5(a). This clearly indicates the presence of biomolecules and bio constituents of *A. vera* extract. A band shift occurs from 1,615 to 1,539 cm^{-1}, which indicates the binding of proteins with the surface of TiO_2 and thereby it leads to the stabilization of NPs. Furthermore, a band shifts from 1,421 to 1,442 and 1,080 to 1,034 cm^{-1} infer the contribution of carboxylic acid and amine groups respectively, which are the capping ligands for the encapsulation of TiO_2 NPs. There is a band shift from 3,423 to 3,372 cm^{-1}, which may be due to the condensation of Ti–OH group. A band at 659 cm^{-1} is attributed to the stretching vibration of TiO_2, as shown in Fig. 5(b). Finally, it can be noticed that the proteins/enzymes, carboxylic acid and amine groups present in the *A. vera* plant extract can lead to the formation of TiO_2 NPs through stabilization and encapsulation respectively [22]. Some of the bands appeared for as-synthesized sample have disappeared after the calcination, as shown in Fig. 5(c).

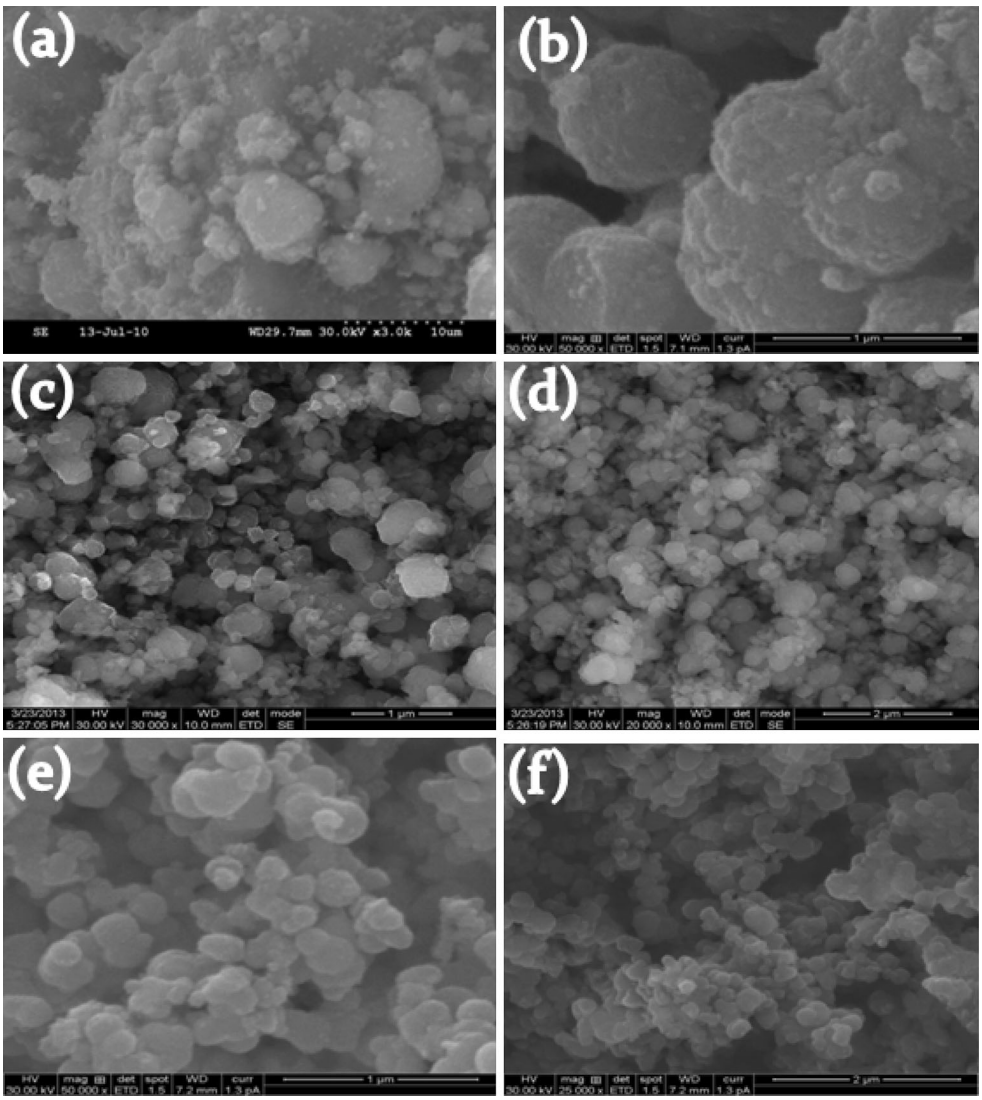

Fig. 6 SEM image of TiO_2 nanopowder calcined at 400 °C. (**a**) Pure TiO_2 without *Aloe vera* plant extract. (**b**) 1AT, (**c**) and (**d**) 2AT, (**e**) and (**f**) 3AT

Figure 6(a) shows the SEM image of pure TiO_2 powder, in which the particles are highly agglomerated due to the simultaneous hydrolysis, condensation and aggregation. It is apparently seen from the Fig. 6(b)–6(f) that the impact of *A. vera* plant extract is clearly observed on the control of agglomeration as well as reduction in particles size of TiO_2 nanopowder. It elucidates the decrease of particles size with the increase of *A. vera* plant extract and also it indicates the spherical shape of the particles. Moreover, the uniformity of the particles (2AT and 3AT) implies the well association of biomolecules with TiO_2 NPs during the synthesis process. In order to ascertain the morphology and particle size (3AT), it has been further subjected to TEM analysis.

The surface area of the TiO_2 nanocorals (3AT sample) calcined at 400 °C has been measured using nitrogen gas adsorption by BET analysis and the specific surface area is 27.6238 m^2/g.

As shown in the TEM image, it perspicuously depicted the presence of plausible nanocorals Fig. 7(a)–7(d) with the diameter in the range of 80–200 nm. It can be clearly visualize that the nanocorals are decorated with the nanopolyps of titanium oxide (TiO_2) having the size in the range between 15 and 30 nm. SAED pattens of the synthesized TiO_2 nanopowder show a polycrystalline nature in Fig. 7(e) and 7(f).

The possible growth mechanism for the resultant TiO_2 cauliflower morphology is still unclear but it is understood on the basis of observed experimental results presented in Fig. 8. As already discussed, the addition of *A. vera* extract results the change of TiO_2 precursor solution from its clear nature to slurry. This indicates the rapid reaction of *A. vera* extract with TiO_2 precursor solution. The growth mechanism may occur in two stages. Firstly, the protein/enzyme–nanoparticle interaction takes place i.e. the protein of the

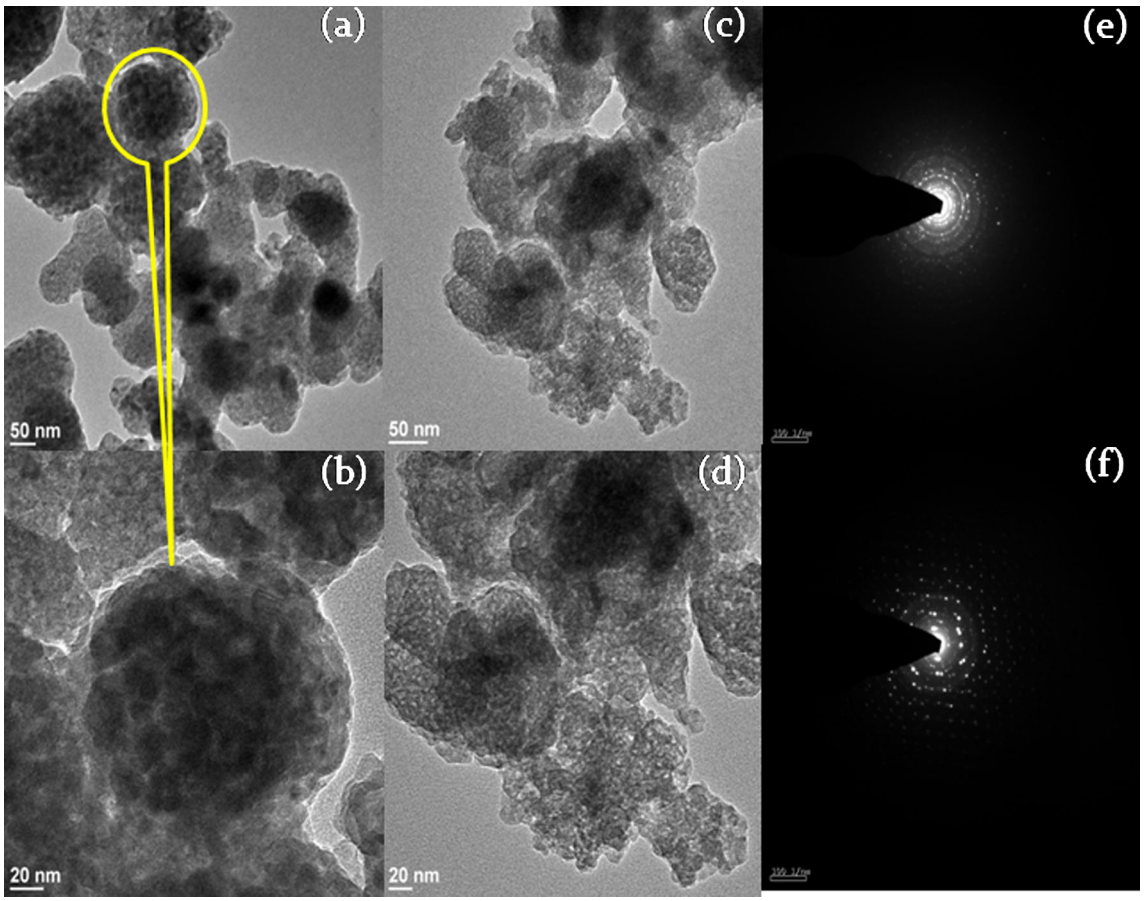

Fig. 7 TEM image of TiO_2 nanocorals calcined at 400 °C. (**a**), (**b**) 3AT, (**c**), (**d**) 1AT, (**e**), (**f**) SAED patterns of 3AT and 1AT

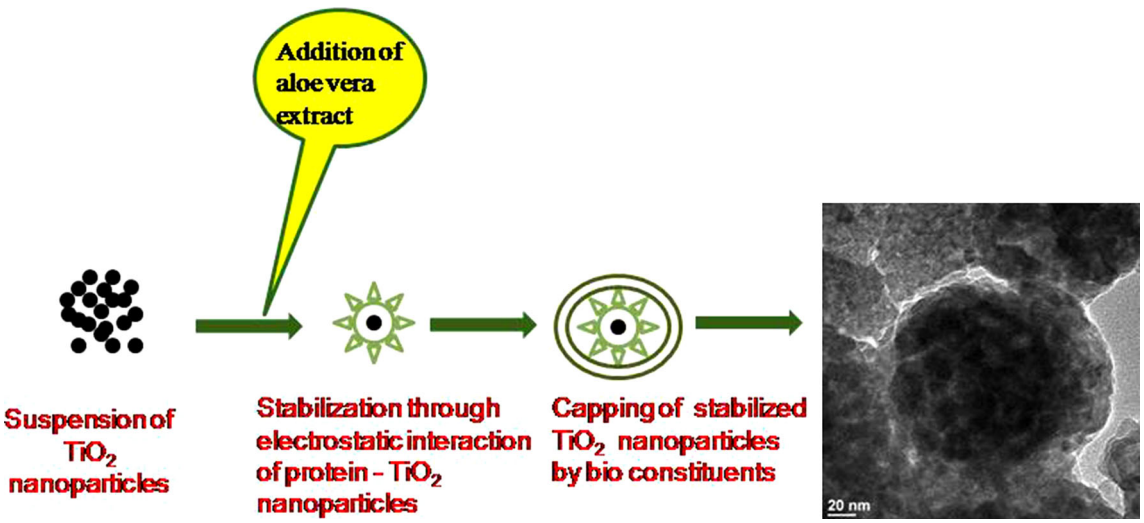

Fig. 8 Schematic illustration of the growth mechaniam of TiO_2 cauliflower-nanocoral morpholgy

A. vera extract can bind with the TiO_2 surface via electrostatic interaction. This is clearly supported by the band shift from 1,615 cm^{-1} to 1,539 cm^{-1} in the FTIR spectrum. In this stage, the aggregation of NPs could be effectively avoided and thus the stabilization of NPs is takes place by proteins, which is supposed to the formation of primary TiO_2 nanopolyps. Secondly, due to the shape-directing ability of carbonyl compounds and other such bio constituents of *A. vera* extract, the capping of TiO_2 nanopolyps stabilized by proteins takes place. During the

calcination at 400 °C, the removal of biological constituents also takes place and the spontaneous aggregation of primary TiO_2 nanopolyps results in the formation of cauliflower-nanocoral morphology. Hence, the formation of TiO_2 cauliflower-nanocoral morphology is due to the synergistic effect of *A. vera* extract.

4. Conclusions

A novel TiO_2 nanocoral architecture is obtained first time using *A. vera* plant extract as a bio-capping agent by sol–gel process. The concentration variation of *A. vera* plant extract enormously changes the particle size of TiO_2 nanopowder and thereby it leads to control the particle size. Thermal analysis reveals the crystallization temperature of 1AT and 3AT at 300 °C. The XRD analysis substantiates the presence of TiO_2 in anatase phase and also the rutile phase of TiO_2 nanopowder (1AT only) at 600 °C for the lower concentration (0.5 ml). Hence the phase transformation of TiO_2 nanoparticle depends on the concentration of *A. vera* plant extract. FT Raman spectra emphasize the presence of TiO_2 anatase phase (3AT) and the Raman band shifts with respect to the particle size variation. The biological molecules are responsible for the formation of TiO_2 NPs, which is analyzed by FTIR spectroscopy. The surface area is measured by BET analysis and it is found to be 27.6238 m^2/g. SEM images depict the homogeneity, formation of TiO_2 NPs with spherical shape and also the reduction of particle size with respect to the concentration of *A. vera* plant extract. Furthermore, TEM images demonstrate the plausible nanocorals decorated with the nanopolyps having the diameter in the range of 15–30 nm.

Acknowledgments The work was financially assisted by University Grants Commission through the scheme of UGC Major Research Project [No. F. 40-74/2011 (SR)] and highly acknowledged. Also, the authors thank School of Physics, Alagappa University, Karaikudi for extending XRD facility and DST PURSE funded HRSEM instrumental facility extended by Department of Industrial Chemistry, Alagappa university, Karaikudi and Indian Institute of Technology (IIT Madras—SAIF) Chennai for extending the FT Raman instrument facility.

References

[1] D R Lide *Handbook of Chemistry and Physics* 71st edn. (Boca Raton: F1 CRC) (1991)
[2] W Q Wu, Y F Xu, C Y Su and DB Kuang *Energy Environ. Sci.* **7** 644 (2014)
[3] W Q Wu, Y F Xu, H S Rao, H L Feng, C Y Su and DB Kuang *Angew. Chem.* **19** 4816 (2014)
[4] W Q Wu, B X Lei, H S Rao, Y F Xu, Y F Wang, C Y Su and D B Kuang *Sci. Rep.* **3** 1352 (2013)
[5] J N Hart, D Menzies, Y B Cheng, G P Simon and L Spiccia *J Sol–Gel Sci. Technol.* **40** 45 (2006)
[6] B Oregan and M A Gratzel *Nature* **353** 737 (1991)
[7] S Sarmah and A Kumar *Indian J. Phys.* **85** 713 (2011)
[8] A Fujishima and K Honda *Nature* **238** 37 (1972)
[9] M R Vaezi, S Khoby Shendy and T Ebadzadeh *Indian J. Phys.* **86** 9 (2012)
[10] S Berger, A Ghicov, Y C Nah and P Schmuki *Langmuir* **25** 4841 (2009)
[11] G Fu, P S Vary and C T Lin *J. Phys. Chem. B* **109** 8889 (2005)
[12] L C Gerhardt, G M R Jell and A R Boccaccini *J. Mater. Sci. Mater. M* **18** 1287 (2007)
[13] H Y Chen, T L Zhang, J Fan, D B Kuang and C Y Su *Appl. Mater. Interfaces.* **5** 9205 (2013)
[14] G Guo, B Yu, P Yu and X Chen *Talanta* **79** 570 (2009)
[15] J Y Liao, B X Lei, H Y Chen, D B Kuang and C Y Su *Energy Environ. Sci.* **5** 5750 (2012)
[16] Z Wang, B Huang, Y Dai, X Zhang, X Qin, Z Li, Z Zheng, H Cheng and L Guo *Cryst. Eng. Comm.* **14** 4578 (2012)
[17] K Eshun and Q He *Crit. Rev. Food Sci. Nutr.* **44** 91 (2004)
[18] M D Boudreau and F A Beland *J. Environ. Sci. Health C* **24** 103 (2006)
[19] J H Hamman *Molecules* **13** 1599 (2008)
[20] S P Chandran, M Chandhary, R Pasricha, A Ahmad and M Sastry *Biotechnol. Prog.* **22** 577 (2006)
[21] Y Zhang, D Yang, Y Kong, X Wang, O Pandoli and G Gao *Nano Biomed. Eng.* **2** 252 (2010)
[22] G Sangeetha, S Rajeshwari and R Venckatesh *Mater. Res. Bullet.* **46** 2560 (2011)
[23] G Sangeetha, S Rajeshwari and R Venckatesh *Prog. Nat. Sci.* **22** 693 (2012)
[24] G Sangeetha, S Rajeshwari and R Venckatesh *Spectrochim. Acta A* **97** 1140 (2012)
[25] P Laokul, V Amornkitbamrung, S Seraphin and S Maensiri *Curr. Appl. Phys.* **11** 101 (2011)
[26] J Klinkaewnarong, E Swatsitang, C Masingboon, S Seraphin and S Maensiri *Curr. Appl. Phys.* **10** 521 (2010)
[27] S Maensiri, P Laokul, J Klinkaewnarong, S Phokha, V Promarak and S Seraphin *J Optoelectron. Adv. Mater.* **10** 161 (2008)
[28] K S Venkatesh, N S Palani, S R Krishnamoorthi, V Thirumal and R Ilangovan *AIP Conf. Proc.* **1536** 93 (2013)
[29] S S Mali, C A Betty, P N Bhosale and P S Patil *Electrochim. Acta* **59** 113 (2012)
[30] R A Caruso, M Giersig, F Willig and M Antonietti *Langmuir* **14** 6333 (1998)
[31] A Golubovic, M Scepanovic, A Kremenovic, S Askrabic, V Berec, Z Dohcevic-Mitrovic and Z V Popovic *J. Sol Gel Sci. Technol.* **49** 311 (2009)
[32] M Niederberger *Acc. Chem. Res.* **40** 793 (2007)
[33] K Porkodi and S D Arokiasamy *Mater. Charact.* **58** 495 (2007)
[34] T Ohsaka, F Izumi and Y Fujiki *J. Raman Spectrosc.* **7** 321 (1978)
[35] M Hudlikar, S Joglekar, M Dhaygude and K Kodam *Mater. Lett.* **75** 196 (2012)
[36] S S Shankar, A Ahmad and M Sastry *Biotechnol. Prog.* **19** 1627 (2003)